DOI: 10.13009/EUCASS2017-155

Experimental Investigation of the VKI Longshot Gun Tunnel Compression Process

Zdeněk Ilich,[⋆†] *Guillaume Grossir,*[⋆] *Sébastien Paris,*[⋆] *and Olivier Chazot*[⋆]
[⋆]*von Karman Institute for Fluid Dynamics*
Chaussée de Waterloo 72, 1640 Rhode-St-Genèse, Belgium
ilich@vki.ac.be · grossir@vki.ac.be · paris@vki.ac.be · chazot@vki.ac.be
[†]Corresponding author

Abstract

The operation of the VKI Longshot hypersonic gun tunnel strongly depends on its compression process by which high-pressure and high-temperature gases are generated in the nozzle reservoir. The main part of this process takes place in a driven tube where a light supersonic piston compresses the test gas nearly adiabatically. In order to provide an experimental database for numerical simulations of the compression process, the present work characterizes this process by means of fast-response pressure sensors fitted at several locations along the driven tube. Moreover, the transient pressure measurements are used to determine the piston motion. Finally, the initial conditions prior to a test and the final reservoir conditions are also monitored.

1. Introduction

The Longshot hypersonic facility (Fig. 1) operated at the von Karman Institute for Fluid Dynamics (VKI) is based on the gun tunnel principle. It enables the partial duplication of hypersonic reentry conditions in terms of Mach and Reynolds numbers, which represents a unique ability across Europe.

The safe and effective operation of the tunnel relies on an operational map which associates the initial conditions to the peak pressure and temperature in the nozzle reservoir. The operational map currently available has been derived from an analytical solution of the Longshot compression process taking place in the driver/driven-tube system.[10] Although this map gives the correct trends, it fails to provide accurate values of the reservoir conditions. Efforts are ongoing to represent the Longshot compression process using a quasi-one-dimensional numerical solver.[6] Experimental data characterizing the compression process are required for validation purposes. They are reported hereafter.

The Longshot facility together with its working principle is described in §2. Temperature and pressure sensors are installed along the driver and the driven tubes to monitor precisely their initial conditions prior to each experiment (§3). Fast-response pressure sensors are then fitted at several locations along the driven tube and the measurements are performed to determine the pressure transients during a test. The motion of the piston is inferred from these pointwise measurements (§4.1). The fast-response pressure sensors are not flush-mounted, due to the thick walls needed to withstand the large pressures involved: instead, a system of pipes and cavities is present. Its influence on measured pressures is evaluated using a quasi-one-dimensional numerical solver (§4.3). The determination of the peak reservoir conditions is discussed in §5.

2. The VKI Longshot wind-tunnel

2.1 General characteristics

The VKI Longshot hypersonic gun tunnel has been described extensively by Grossir.[5] It allows for experiments at high Mach numbers and at relatively large Reynolds numbers in low-enthalpy environments. The sketch of the wind tunnel is given in Fig. 1 together with a description of its main parts: the driver tube, the driven tube where a piston moves, and the test section with a hypersonic nozzle.

The system of the driver/driven tubes is used to generate high pressures and temperatures in the reservoir of the nozzle. The maximal reservoir pressure and temperature currently achieved are on the order of 400 MPa and 2 500 K.

DOI: 10.13009/EUCASS2017-155

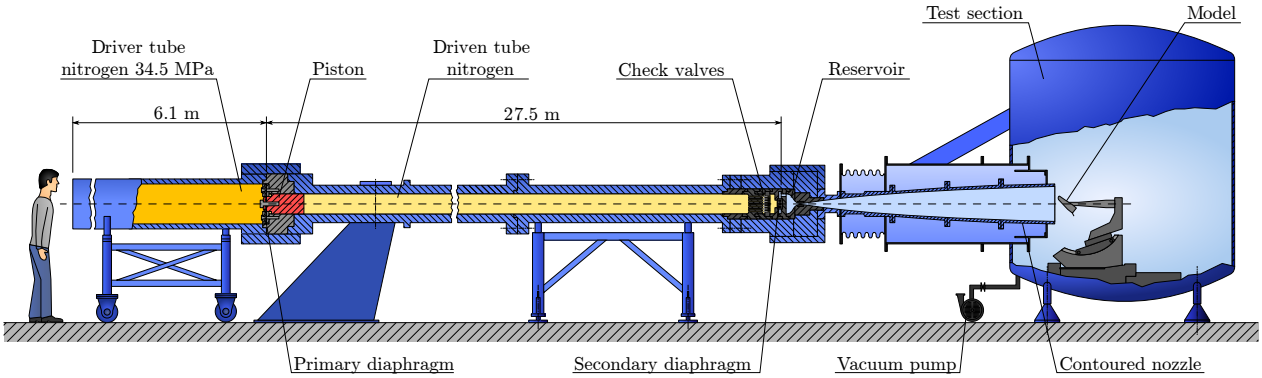

Figure 1: Sketch of the VKI Longshot hypersonic gun tunnel.

The corresponding total enthalpy is still rather low ($h_0 < 3.4\,\mathrm{MJ/kg}$) so that no dissociation effects are present providing nitrogen is used.

The gas trapped in the reservoir is then expanded through contoured or conical nozzles. Stagnation conditions are decaying with time because of the mass flow out of the finite-volume reservoir. The temporal decay of corresponding free-stream flow properties is sufficiently slow in most instances to consider the flow as a succession of quasi-steady events, as demonstrated by Grossir.[5] Therefore, a single experiment in the Longshot wind tunnel offers the possibility to scan a range of Reynolds numbers, increasing its productivity.

2.2 Working principle

The compression cycle of the Longshot wind tunnel has been analyzed theoretically[4,10] and more recently also numerically.[2,6] The piston is set in motion by the controlled rupture of the primary diaphragm and by the large pressure difference existing between the driver and the driven tubes[a]. Its typical acceleration is on the order of $10^5\,\mathrm{m/s^2}$. Shortly after the release of the piston, compression waves focus and generate a shock wave ahead of the piston. The piston quickly approaches its final velocity, traveling within the driven tube at about $600\,\mathrm{m/s}$. This compresses nearly adiabatically the test gas located ahead.

The primary shock wave is reflected several times between the end of the driven tube and the front face of the piston, thereby increasing the test gas temperature and rapidly slowing down the piston with peak deceleration on the order of $10^6\,\mathrm{m/s^2}$. The secondary diaphragm, which initially separates the driven tube from the test section (vacuumed prior to a test), bursts under the large pressure difference allowing the gas to fill the nozzle reservoir located downstream (Fig. 2). Once the kinetic energy of the piston has been entirely converted into the enthalpy of the test gas, the maximum peak pressure and temperature are achieved in the reservoir. The set of 48 small check valves, located at the end of the driven tube, traps the gas at the largest stagnation conditions and prevents it from flowing back to the driven tube once the piston rebounds. These peak stagnation conditions are then used for testing purposes as the trapped gas expands through the nozzle.

The state-of-the-art analysis and description of the Longshot compression process can be found in Grossir at al.[6]

2.3 Initial conditions

In the VKI Longshot wind tunnel, the reservoir stagnation conditions resulting from the compression process can be adjusted by three independent parameters: the initial pressure in the driver tube, the initial pressure in the driven tube, and the mass of the piston.

Three different combinations of these parameters are used regularly. These are namely the “Low”, “Medium” and “High” Reynolds number test conditions listed in Table 1. For each, the approximate range of free-stream unit Reynolds numbers is indicated following the most recent calibration of the wind tunnel[5] (a range of Mach and Reynolds numbers is stated because flow conditions evolve with time). The Mach number variation is explained by the different area ratio of the nozzle induced by the decaying Reynolds number and the varying boundary-layer displacement thickness. Additional test conditions can be obtained using different combinations of these three independent initial parameters.

[a] The larger diameter of the driver with respect to the driven tube creates a chambrage effect, well described by Seigel,[9] which benefits to the work done on the piston by the driver gas.[4,8]

DOI: 10.13009/EUCASS2017-155

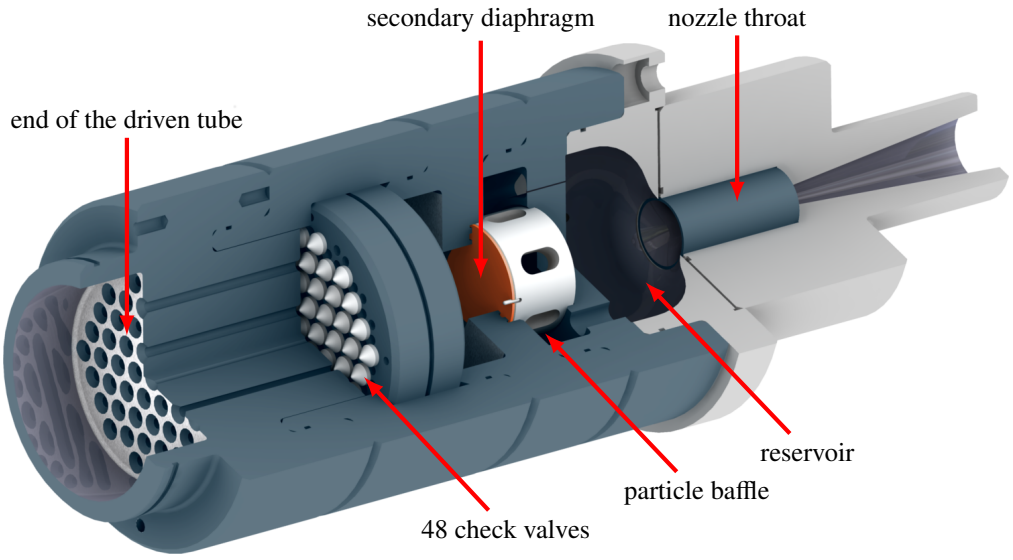

Figure 2: Longshot check valve system at the end of the driven tube.

Table 1: Initial conditions commonly used for the operation of the Longshot wind tunnel with its contoured nozzle.

	"Low Re."	"Medium Re."	"High Re."
Driver tube pressure	34.5 MPa	34.5 MPa	34.5 MPa
Driven tube pressure	144.1 kPa	235.4 kPa	275.8 kPa
Piston mass	1.59 kg	3.215 kg	4.58 kg
Free-stream Mach number	9.5–11	10–12	10–12
Free-stream unit Reynolds number	$3–6 \cdot 10^6$ /m	$6–12 \cdot 10^6$ /m	$7–13 \cdot 10^6$ /m

3. Measurements of initial conditions

3.1 Temperature measurements

Standard type K thermocouples (Chromel-Alumel) have been installed along the driver and the driven tubes to measure the initial temperature of the gases. These measurements are performed through existing ports (R6 and N7 are used for the driver and driven tubes, respectively, Fig. 4). Fig. 3 depicts the thermocouple assembly. The wires of the thermocouples are glued inside a Plexiglas tube while the junction is made at its end, next to the inner diameter of either the driver or the driven tubes. The enlarged base of the tube is held in position as indicated in Fig. 3a using a screw at its back. Proper sealing is ensured by a conical piece.

Temperatures are monitored continuously at a low sampling rate (typically 10 Hz). These initial temperature measurements reveal the driven gas to be near the ambient temperature. The driver gas exhibits larger variations (due to residual heat from compressors) but their amplitude remains limited to about 3% above the ambient one.

3.2 Pressure measurements

Pressure measurements in the driver and the driven tubes prior to a test are currently performed using different types of gauges which are part of an automation system operating the tunnel.

In the driver tube, the nominal pressure is 344.7 bar. It is monitored by a pressure sensor Honeywell A-5 with pressure range up to 1379 bar.

In the driven tube, the pressure typically varies between 1.4 – 3 bar depending on the test conditions to be achieved. It is measured using an absolute WIKA S-20 pressure sensor (10 bar range).

DOI: 10.13009/EUCASS2017-155

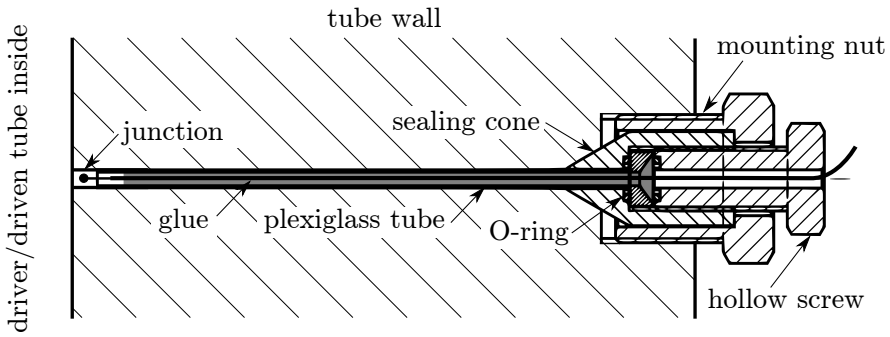

(a) Technical drawing.

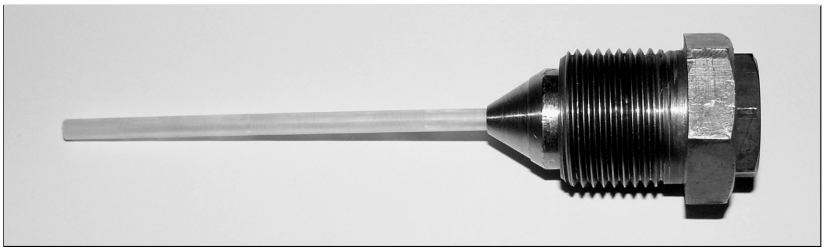

(b) Assembly in which a type K thermocouple will be glued.

Figure 3: Thermocouple assembly in ports of the driver/driven tubes for measurements of the initial temperatures.

4. Characterization of the compression process

4.1 Pressure measurements along the driven tube

4.1.1 Instrumentation

The driven tube of the Longshot wind tunnel is equipped with 8 ports along which instrumentation can be installed. The location of these ports along the driven tube is indicated in Fig. 4 and summarized in Table 2. For each port location, two access points 180° apart are available. The inner diameter of these ports is limited to 4.76 mm (3/16 in) so that instrumentation such as pressure sensors usually need to be mounted recessed by about 45 – 120 mm depending on the local thickness of the driven tube.

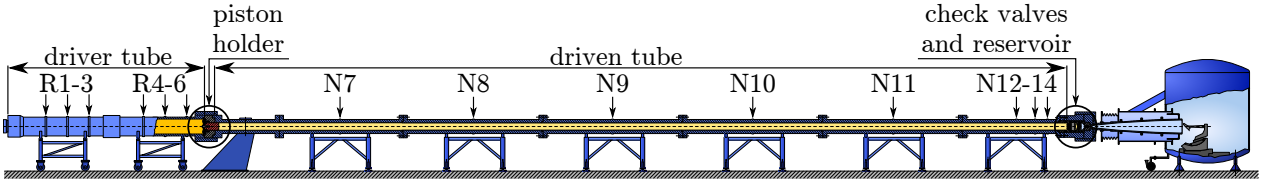

Figure 4: Available ports along the driver and the driven tubes.

Six of these ports have been instrumented with various Kistler piezoelectric pressure transducers as indicated in Table 2 using adapters described in Fig. 5. Depending on the expected pressure range at each location, different types of sensors have been used: old 6201B near the driver/driven interface, 601H along the driven tube, and 6215 towards the end of the driven tube where the largest pressures occur. Sensors are connected to a Kistler 5165A conditioner and sampled at 500 kHz using the Longshot data acquisition system.

The transducer calibrations provided by the manufacturer are used with reported accuracy of 2.2 bar and 15 bar for the types 601H and 6215, respectively.

4.1.2 Measurements

The fast-response pressure sensors newly available enable quantitative measurements of the transient pressure during the compression process at few locations along the driven tube. These can be used to validate numerical predictions.

DOI: 10.13009/EUCASS2017-155

Table 2: Instrumentation ports available along the driven tube.

Port[b]	Distance from primary diaphragm	Instrumentation
N7	5.3363 m	(Kistler 6201B)
N8	9.6035 m	-
N9	13.8707 m	Kistler 601H
N10	18.1379 m	-
N11	22.4051 m	Kistler 601H
N12	26.0627 m	Kistler 601H
N13	26.8247 m	Kistler 601H
N14	27.2057 m	Kistler 6215

[b]Ports along the driver tube (R1 – R6) are not used here.

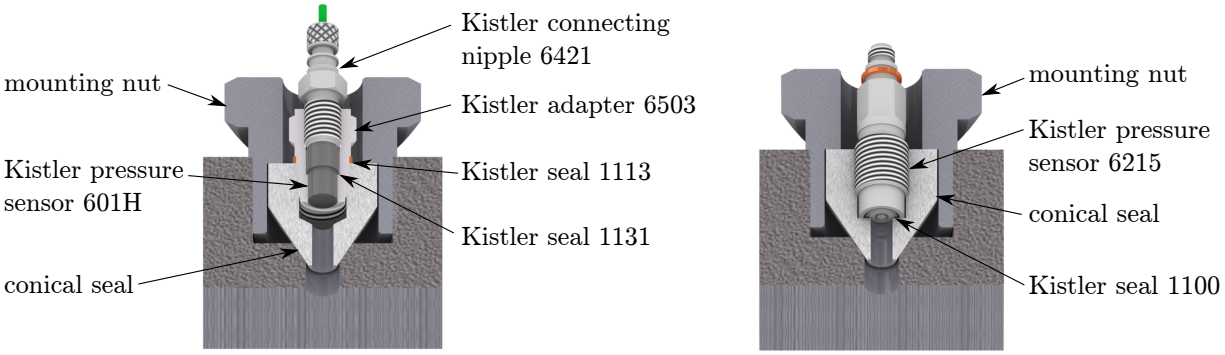

(a) Kistler 601H.

(b) Kistler 6215.

Figure 5: Assembly of pressure sensors in ports of the driven tube.

In addition, peculiar events (e.g. shock waves, expansions waves, piston passage...) can be identified and used to infer an approximate trajectory of the piston and paths followed by compression/expansion waves.

Two different operating conditions have been investigated approximately corresponding to Low and Medium Reynolds regimes. Their initial conditions are detailed in Table 3. Typical results are reported in Figs. 6 and 7 for which the reference time is chosen as the instant when the piston is released, indicated by the accelerometer mounted on the driven tube. Characteristic events for the experimental pressure traces are labeled as follows:

- event 1: primary shock wave,
- event 2: first reflection (from the end of driven tube),
- event 3: second reflection (from the front face of the piston),
- event 4: third reflection (from the end of driven tube),
- event 5: fourth reflection (from the front face of the piston),
- event 6: *piston* passage,
- event 7: upstream traveling shock due to piston rebound,
- event 8: second *piston* passage.

Based on each major event of the pressure profiles, space-time ($x-t$) diagrams representing the trajectory of the piston as a function of time can be established. An example of such a diagram is given in Fig. 8 for an experiment at low Reynolds number.

The initial part of the trajectory can only be characterized from port N7. This means that the initial profile of the trajectory and the acceleration of the piston remain unknown. Due to improper behavior of the old sensor 6201B used

DOI: 10.13009/EUCASS2017-155

Table 3: Longshot initial conditions for the presented tests using a conical nozzle.

	p_{driver}	p_{driven}	m_{piston}
Low Reynolds test	$345 \cdot 10^5$ Pa	$1.441 \cdot 10^5$ Pa	1.488 kg
Medium Reynolds test	$345 \cdot 10^5$ Pa	$2.354 \cdot 10^5$ Pa	3.204 kg

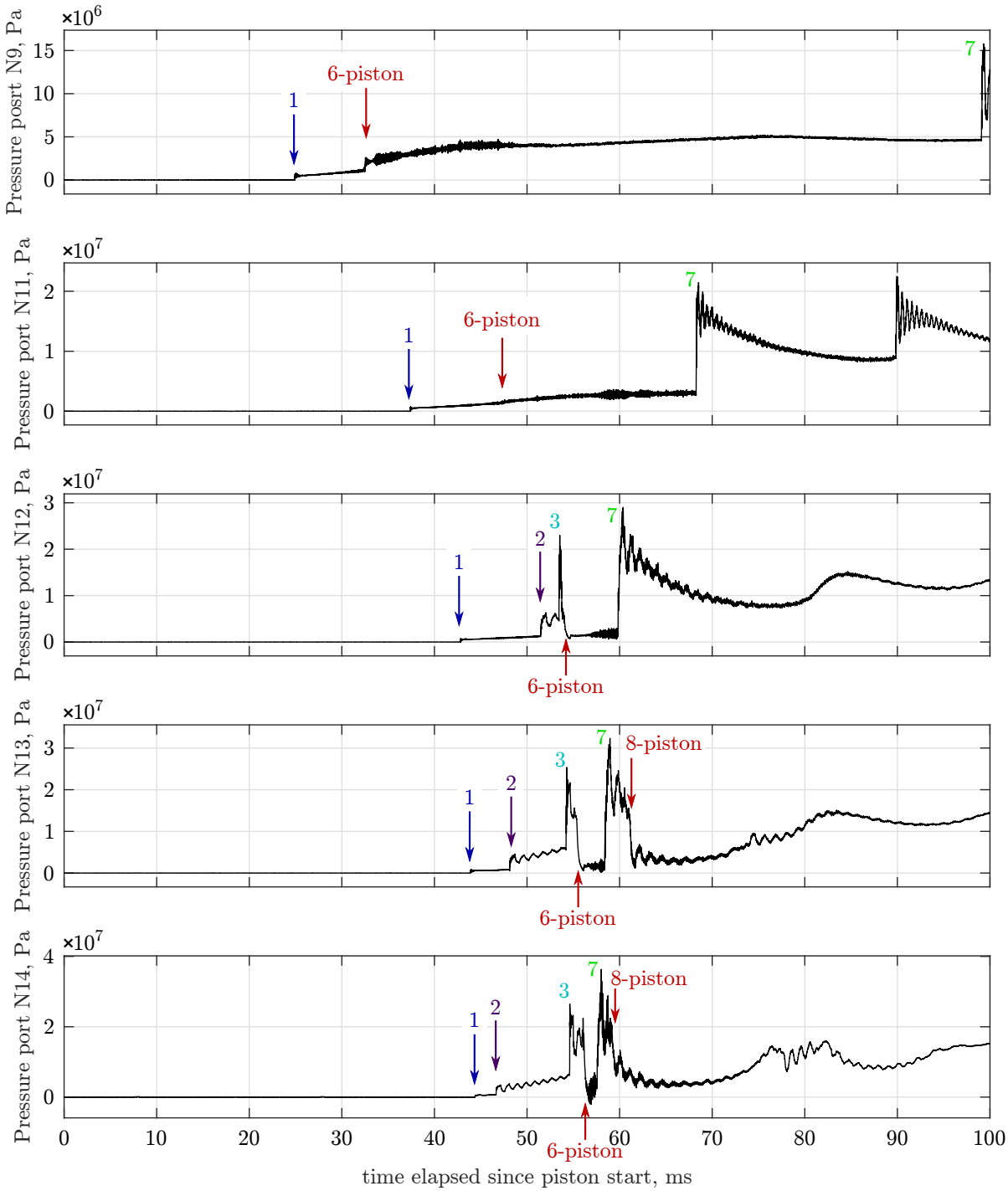

Figure 6: Pressure at different locations along the driven tube, which correspond to Fig. 4. The numbers indicate characteristic events. Low Reynolds test.

DOI: 10.13009/EUCASS2017-155

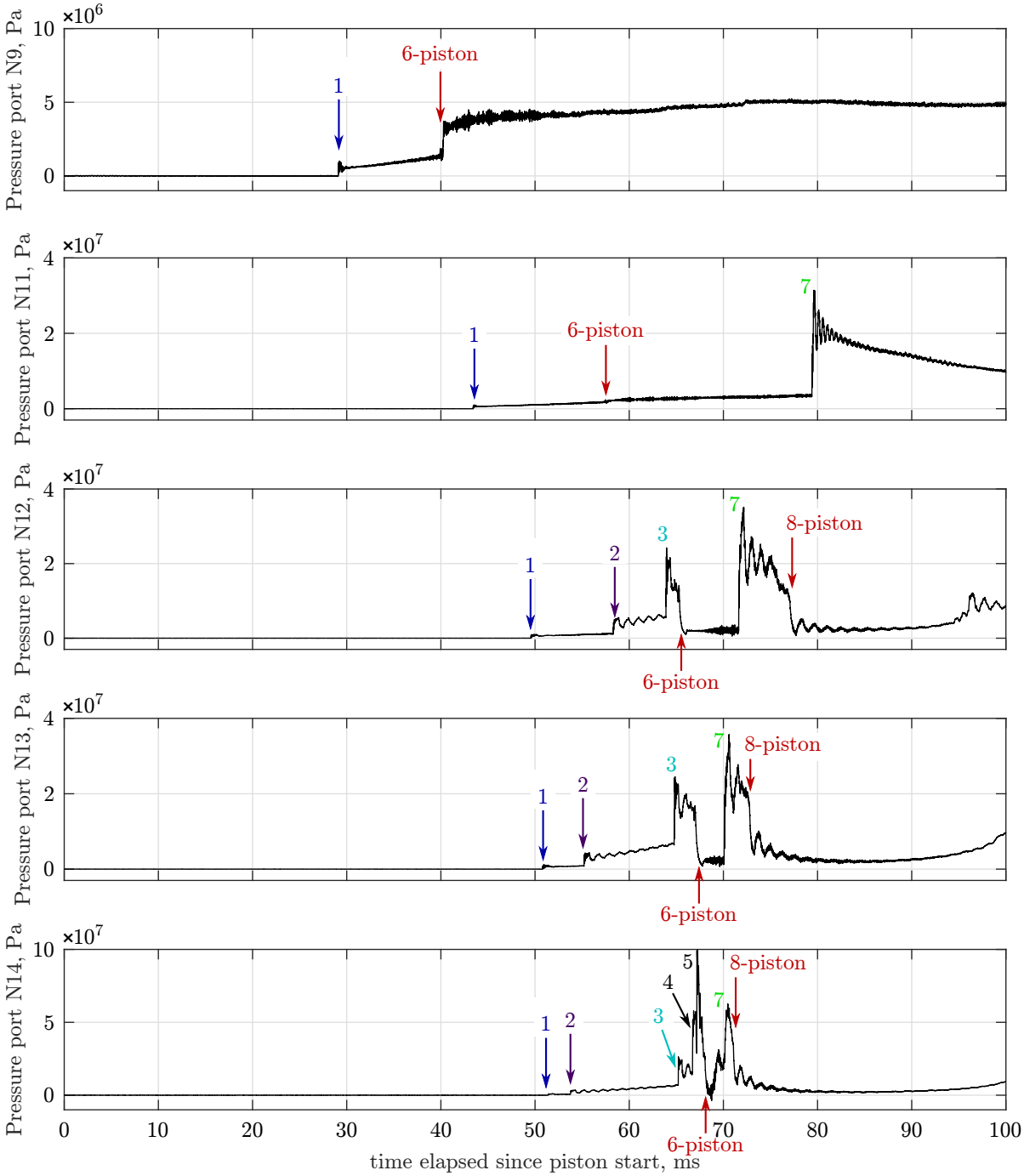

Figure 7: Pressure at different locations along the driven tube, which correspond to Fig. 4. The numbers indicate characteristic events. Medium Reynolds test.

DOI: 10.13009/EUCASS2017-155

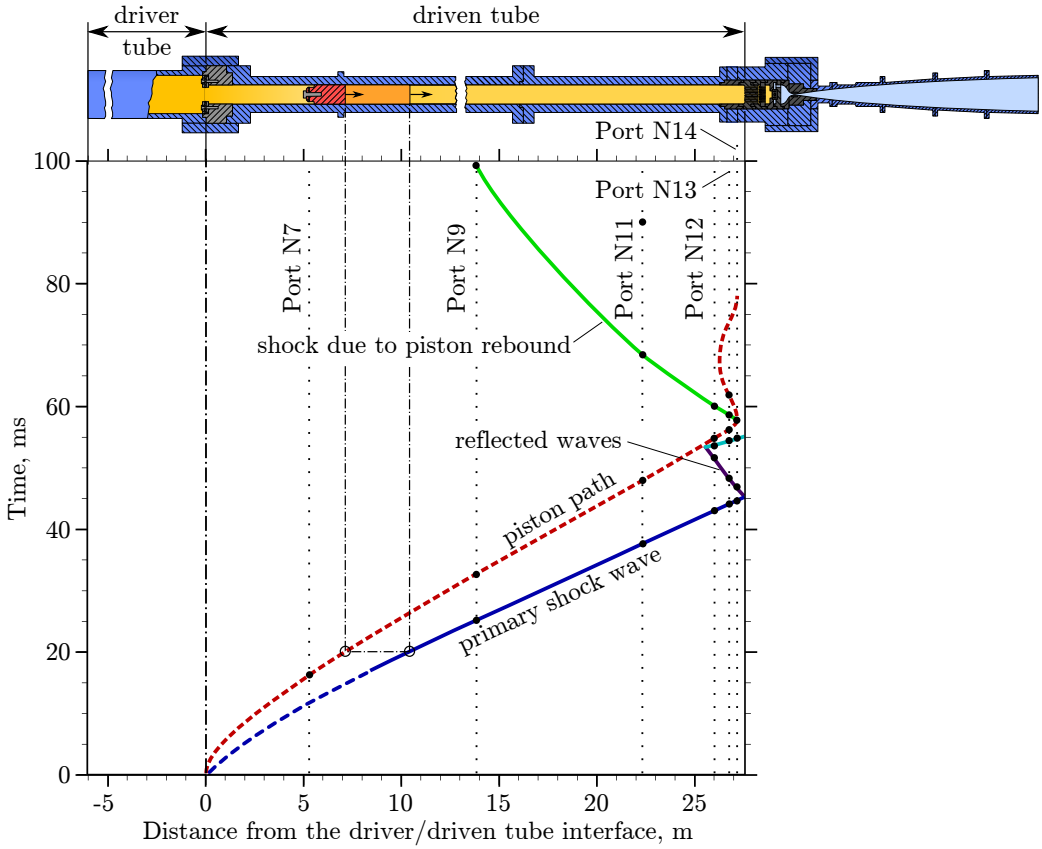

Figure 8: Space-time diagram derived from pressure measurements along the driven tube (Low Reynolds test). Symbols • denote characteristic events from the pressure traces. The layout of the driver/driven tube system is not to scale for clarity.

for the first port, no reliable pressure traces have been obtained for this location. The acquired signals can serve only as indicators of the characteristic events.

In between ports N7 and N11, only one sensor is available but the trajectory is essentially uniform so that it can be well approximated. The path followed by the primary shock wave (identified with the label #1) traveling faster than the piston can also be drawn.

The interpretation of the results is more difficult towards the end of the driven tube (in spite of many sensors), because of the numerous events which take place in a short time. The first series of reflections of the primary shock wave by the end of the driven tube towards the piston and back is clearly observed for both tests (labels #2 and #3). Another series of reflections can also be distinguished for the Medium Reynolds test (labels #4 and #5).

As the piston goes beyond the last port N14 (located 475.5 mm before the end of the driven tube), the measurement corresponds to the driver gas behind the piston. The rebound of the piston then induces the shock wave traveling upstream the driven tube (label #7). For the Medium Reynolds test, the rebound is stronger and the second piston passage is observed also in port N12, unlike for the Low Reynolds test where the rebound is limited to two last ports. However, the precise trajectory of the piston near the end of the driven tube remains unknown with the limited number of ports available.

The event from port N11 at time instant about 90 ms, which is not related to any theoretical phenomena of the compression process in Fig. 8, is probably caused by a second piston rebound. The latter generates a pressure wave that forms a shock later on. A number of piston rebounds, and thus a number of shocks traveling upstream, is typically equal to 3 for the Low Reynolds regime[c].

4.2 Quasi-1D numerical solver

The current modeling of the Longshot compression process[6] relies on the L1d code developed by Jacobs from the University of Queensland (Australia).[7] It is a quasi-one-dimensional Lagrangian solver where the space discretization

[c]It was observed for another experiment at Low Reynolds number using long acquisition time.

DOI: 10.13009/EUCASS2017-155

of gas slugs is performed only along the longitudinal coordinate using a number of cells (control-mass elements) but gradual changes of the tube diameter can be taken into account. The gas-dynamics is based on a control-mass formulation which tracks interface positions of the gas cells. The pressure and the velocity at each interface are computed via a local Riemann problem. Piston dynamics is coupled to the gas dynamics by using the piston velocity as a boundary condition to the gas slugs and then using the computed gas pressure as the forcing term in the piston dynamics.

The original version of the L1d code available at the VKI has been customized to allow its use for the determination of the operational map. Up to now, several improvements have been brought to the code. The crucial ones were among others:[6]

- use of the real-gas equation of state via the Span & Wagner equations for nitrogen,
- identification of suitable correlations for the viscosity effects and for the bore friction between tube and piston.

The comparison of pressure profiles between the state-of-the-art numerical simulation and the experiment is shown for the Medium Reynolds test in Fig. 11a and 12a for ports N9 and N13, respectively. Note that discrepancies occurring after the piston rebound (at ≈68.6 ms) are expected as the numerical simulations do not model the closure of the check valves.

4.3 Evaluation of the cavity effect

4.3.1 Cavity geometry

It has been pointed out in §4.1.1 that the pressure sensors are not flush-mounted to the inner surface of the driven tube. Due to the presence of a cavity in between the driven tube and the sensor, the acquired pressure traces may not correspond to the actual pressure variations inside the tube. To evaluate this distortion of the measured pressures, the unsteady response of the measuring system including connecting lines, cavities and a sensor itself must be determined either by time domain analysis (utilization of a pressure step) or by frequency domain analysis (utilization of a sinusoidally varying pressure of adjustable frequency). Since the events in measured traces have a character of the pressure step, the step response of the cavities is of primary interest. The most important effects resulting from such analysis are the time delay (affecting the position of points in space-time diagrams) and the magnitude of oscillations or wiggles in the pressure traces.

Varying wall thicknesses along the driven tube and different types of pressure sensors lead to three configurations of the connecting system (excluding sensor 6201B at port N7). Their simplified geometry is represented in Fig. 9. The dead volume of the sensors themselves has been accounted for (≈10 mm^3). However, this volume is assumed to be constant since its change caused by deformation of the sensor diaphragm is negligible.

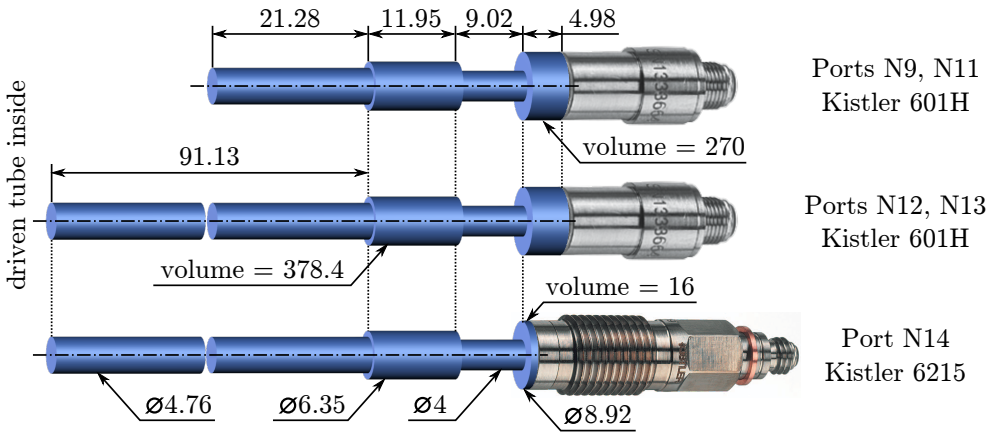

Figure 9: Volume distributions of the connecting system for different ports along the driven tube (dimensions in mm and mm^3).

DOI: 10.13009/EUCASS2017-155

4.3.2 Small disturbance approach

A classical theory deriving the step response for such a system consisting of multiple tubes and volumes has been developed by Bergh and Tijdeman.[3] This theory predicts the response in the frequency domain, which is then translated into a prediction of the step response. The main assumption is that pressure steps must be small compared to absolute pressures.

Attempts to determine the cavity effect for the present case failed mainly due to a limited range of applicability of that theory – the maximal pressure amplitudes reach values on the order of 50 MPa (Figs. 6, 7). The frequencies of oscillations were overestimated by as much as 50% against experimental observations. Therefore, it is concluded that this simple approach cannot be used to accuratelly describe the responce of the cavity in the present case. Instead, a numerical solver can be used.

4.3.3 Numerically determined step response

The L1d code (described in §4.2) is used also to determine flow inside the cavity exposed to the pressure step. For that purpose, a cylinder with a diameter of 39 mm and a length of 76.2 mm (corresponding to an internal diameter of the real driven tube) is attached to the original geometry of the cavity (Fig. 9). This cylinder having sufficiently larger volume compared to the cavity itself (more than 37 times) represents the driven tube in the vicinity of a port.

The initial conditions (pressure and temperature) for the simulation are set according to the numerical results of the whole compression process mentioned in §4.2. An example of the simulation setup is illustrated in Fig. 10. The thermal and transport properties of nitrogen are determined as in Grossir et al,[6] namely using the Span & Wagner real gas equations of state and the Sutherland law for the dynamic viscosity. The convective heat transfer to the tube wall is determined using Reynolds analogy for turbulent flows in pipes.

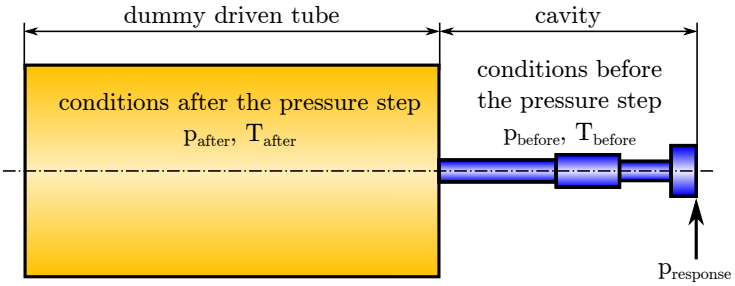

Figure 10: An example of geometry used for the numerical evaluation of the cavity effect with settings of initial conditions.

The results are presented for two characteristic events of the Medium Reynolds test covering different ranges of pressures and temperatures before and after the step. These are namely the primary shock (label #1 in Fig. 7) from port N9 (Fig. 11b), and the second reflection (label #3 in Fig. 7) from port N13 (Fig. 12b).

Both examples show that the numerical simulations of the cavities are able to accurately reproduce, at least for a limited time after the step, the low-frequency oscillations and the harmonics observed experimentally. The discrepancies occurring afterward can be attributed to the different evolution of the pressure inside the real and the dummy driven tubes. This can be assessed in Fig. 11b and 12b by comparing the pressure after the step (p_{after}) with the results of the L1d simulations of the whole compression process. Therefore, it can be concluded that the sensors themselves play a minor role[d] on the observed wiggles in experimental pressure traces, and that the cavity is the prime responsible.

In principle, such simulations can be carried out for every characteristic event (except the piston passage) for each port along the driven tube in order to determine the time delay which should be considered when the space-time diagrams are plotted. This time delay introduced by the cavity effects is for the standard Low and Medium Reynolds regimes on the order of 0.1 – 0.3 ms depending on the length of the tube and on the local flow temperature. Practically, only the worst scenario corresponding to the largest cavity (ports N12 and N13) and lower temperature (primary shock) is commonly evaluated and the corresponding time delay is included to the measurement uncertainties.

It should be noted that a correction of the measurements based on a transfer function is difficult because the cavity response changes depending on pressures and temperatures involved. These vary significantly in time even for one specific location (port) as shown in Figs. 11a and 12a for pressures and in Figs. 13a and 13b for corresponding

[d]The natural frequency for Kistler sensors 601H and 6215 are ≈150 kHz and >240 kHz, respectively.

DOI: 10.13009/EUCASS2017-155

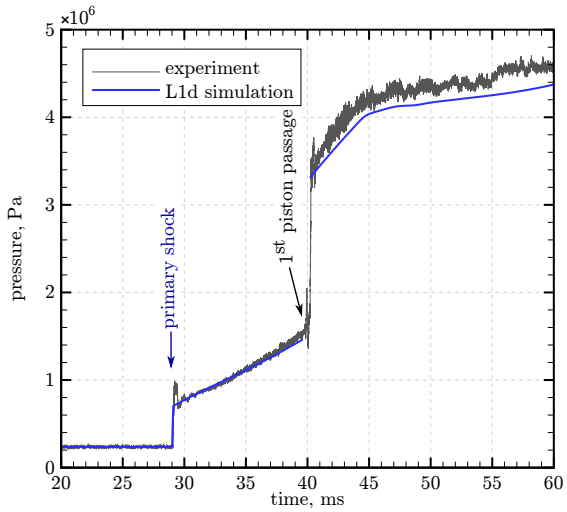

(a) Experiment vs. L1d simulation of whole compression process.

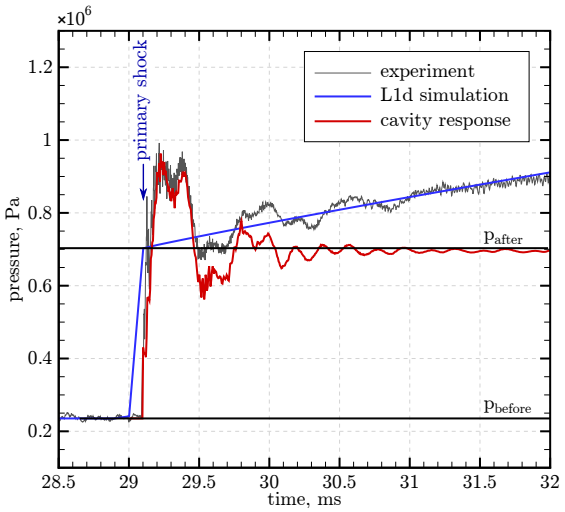

(b) Detail of the primary shock (experiment and L1d simulation) together with numerically determined pressure step response of the connecting cavity.

Figure 11: Pressure profile from port N9 for the Medium Reynolds test.

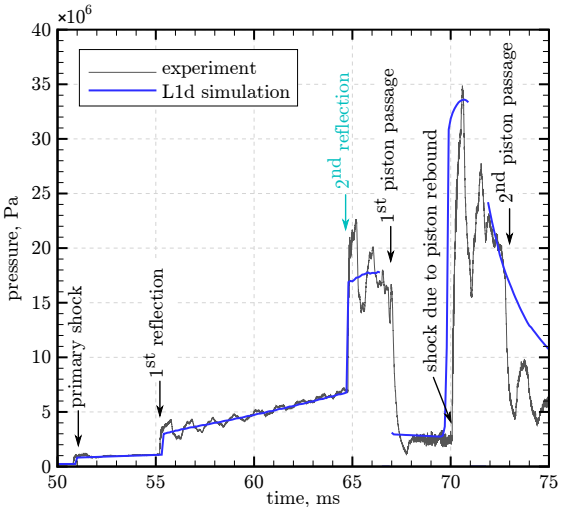

(a) Experiment vs. L1d simulation of whole compression process.

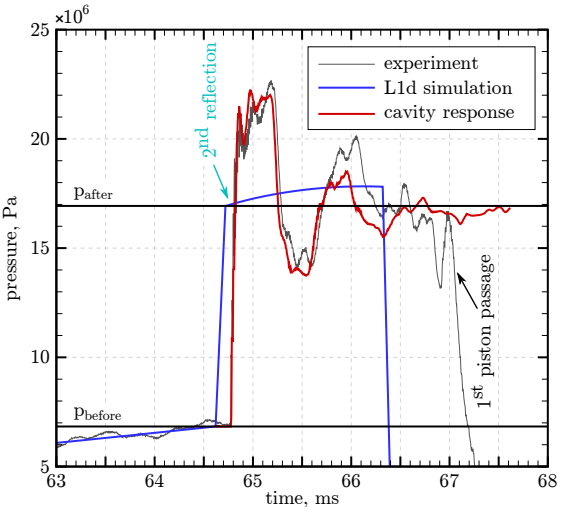

(b) Detail of the second reflection (experiment and L1d simulation) together with numerically determined pressure step response of the connecting cavity.

Figure 12: Pressure profile from port N13 for the Medium Reynolds test.

temperatures resulting from the L1d simulations of the whole compression process[6] (no unsteady measurement of temperature evolution is currently available).

5. Determination of peak reservoir conditions

Although the reservoir conditions (pressure and temperature) are no longer used for the determination of the free-stream conditions in the test section,[5] they represent a valuable information for the assessment of the repeatabilities between successive experiments and for the validation of numerical simulations. However, there is currently no method available for the Longshot tunnel to directly measure the *reservoir temperature*. Difficulties associated with utilization of thermocouples in the reservoir have been discussed by Backx.[1]

Pressure measurements in the reservoir are performed using a fast-response Kistler pressure sensor (Kistler 6215). The sensor is again mounted in a recessed cavity, which introduces wiggles on the measurements (at about $1 - 2$ kHz), as illustrated in Fig. 14. Therefore, the maximal pressure measured by the sensor does not correspond to a realistic peak pressure in the reservoir. The currently used approach to determine this realistic peak pressure from the measured

DOI: 10.13009/EUCASS2017-155

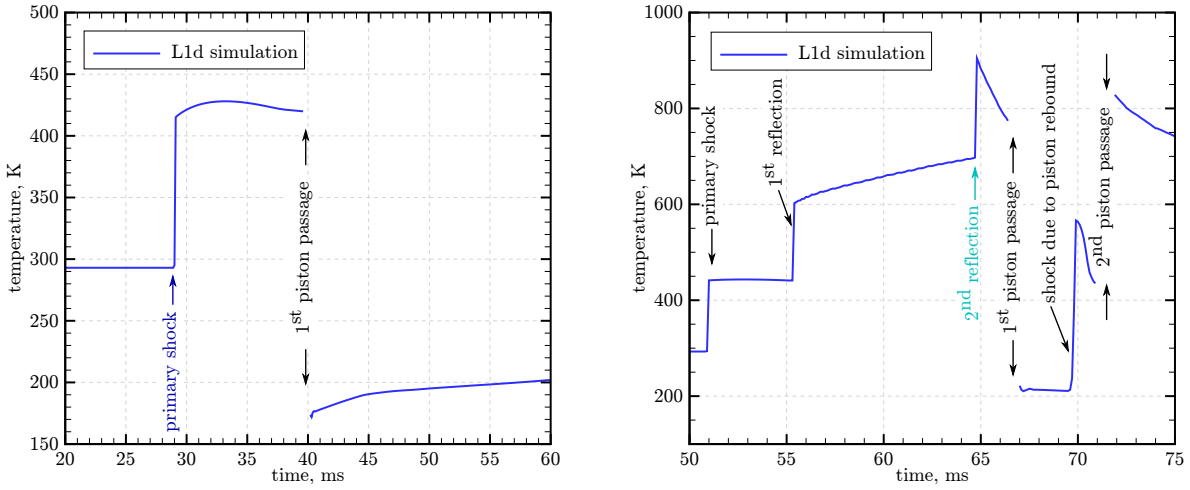

(a) Port N9. (b) Port N13.

Figure 13: Temperature profiles resulting from L1d numerical simulations of the whole compression process, Medium Reynolds test.

traces relies on a fitting method, which is described hereafter.

The first step is to appropriately define the time instant of the beginning of an experiment, i.e. $t = 0$ ms. This zero time is selected as the time instant when the measured reservoir pressure reaches half of its maximum (as done in Figure 14). This corresponds to a steep increase which is therefore closely associated with the peak reservoir conditions.

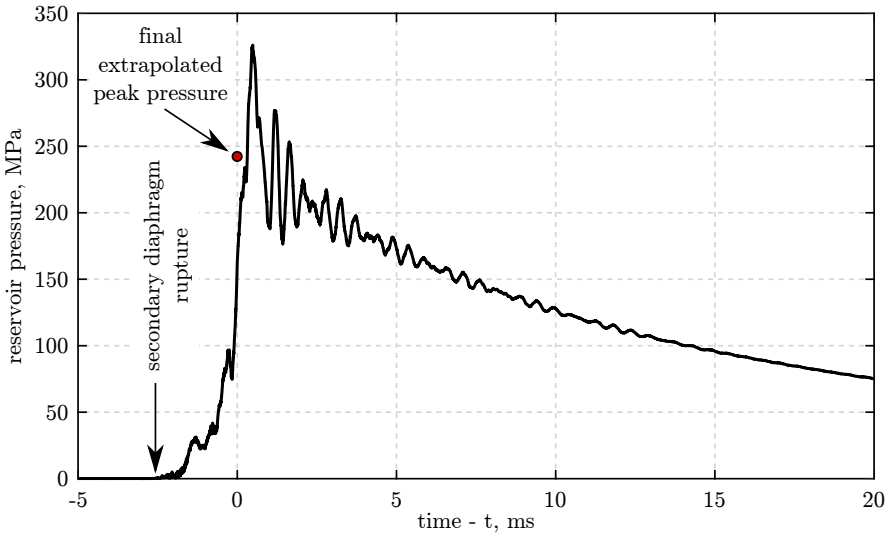

Figure 14: Typical pressure measurement in the Longshot reservoir, Medium Reynolds test.

Due to the flow out of the finite-volume reservoir, the pressure approximately follows an exponential decay from the peak value. Therefore, this desired peak is determined by fitting the logarithm of the measured pressure (a polynomial of degree 2 is commonly used as the decay is not perfectly exponential) in the time range from t_1 to t_f and by a subsequent extrapolation to $t = 0$ ms.

Such an extrapolated peak value is, however, sensitive to the choice of the time interval $[t_1, t_f]$ used for the fitting. In order to enhance the robustness, a series of fits with the fixed maximal time t_f (corresponding to the useful test time) and the varying starting time t_1 is actually performed. Each fit leads to a different extrapolated value which is plotted in Fig. 15 versus the corresponding starting time t_1. After initial oscillations ($t_1 \approx 1$ ms in Fig. 15), it is possible to recognize a part where extrapolated values oscillate around a linearly varying mean[e]. As the time t_1 moves

[e]Note that the nearly constant trend of that linear part observed in Fig. 15 is rather rare and should be considered as fortuitous.

DOI: 10.13009/EUCASS2017-155

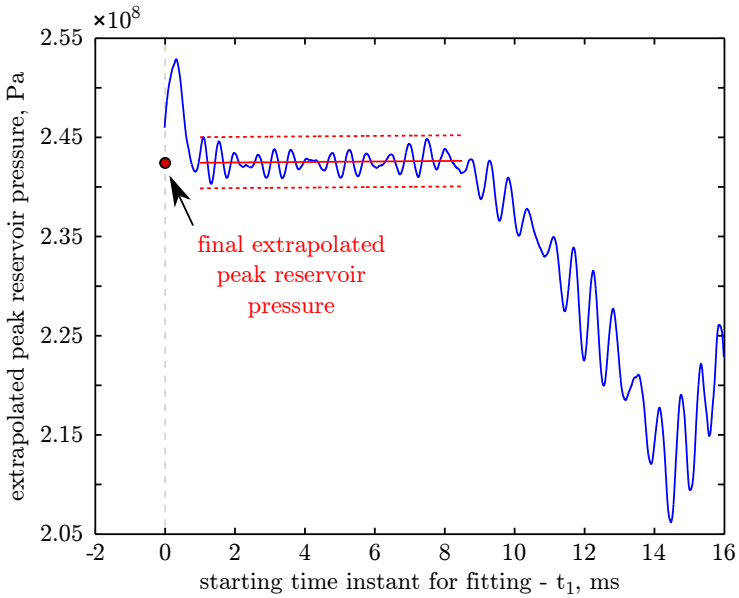

Figure 15: Illustration of the method used to determine the peak pressure in the reservoir.

further from the zero time, the extrapolations are no longer accurate and the departure from the linear part is observed (at $t_1 \approx 8.5$ ms in Fig. 15).

The last step of the procedure is the determination of the final peak reservoir pressure using a fit of the linear part in Fig. 15 and the subsequent extrapolation of this fit to $t_1 = 0$ ms. This peak pressure is used as an experimental reference (also depicted in Fig. 14). Combined uncertainties from the curve fit procedure and the sensor accuracy lead to an accuracy of $\pm 1\%$.

Note that, in principle, the same numerical analysis of the cavity effects as discussed in §4.3 can likely be performed, at least to check whether the determined peak pressure agrees with oscillations observed in the measured signal. However, for the case of the reservoir, such a numerical simulation would be more expensive, not only due to the larger pressures and temperatures involved, but mainly due to complex series of events taking place in the reservoir prior to the main pressure step. After the rupture of the secondary diaphragm (Fig. 14), typically caused by the impact of the second reflected shock (label #3), the shock is propagated through the particle baffle into the reservoir followed by series of shock reflections. This behavior is clearly visible in the first part of Fig. 14 after the rupture of the secondary diaphragm.

6. Conclusions

Experimental data characterizing the compression process of the Longshot hypersonic tunnel has been presented and discussed.

The addition of the initial pressure and temperature measurements reduced uncertainties on the initial conditions. This has uncovered that a commonly used assumption of equality between initial temperatures inside the tubes and ambient one is valid only for the driven tube, whereas the initial temperature in the driver tube can be about 10 K higher due to the specific filling process.

The fast-pressure measurements have improved the characterization of the compression process and provide valuable data for validation of the numerical simulations. It has been shown that oscillations presented in the measured pressure signals are mainly due to the cavity effects and not to the sensors themselves. This eases identification of typical events in the pressure signals (e.g. shock waves, reflected shocks, piston arrivals). Therefore, the partial determination of the piston trajectory is also enabled by these pointwise pressure measurements, except by the end of the compression process, where no instrumentation ports are available. Complementary diagnostics will be required for determining the rebounding point of the piston. The typical time delay on the experimental data due to the cavity is on the order of $0.1 - 0.3$ ms.

At last, the determination of the reservoir conditions, which result from the compression process, has been discussed and the common procedure of the evaluation of the peak reservoir pressure has been described.

The present set of reliable experimental data gives the sound basis for the successful numerical simulations of the compression process in the VKI Longshot hypersonic facility and thus contributes to its more effective operation.

DOI: 10.13009/EUCASS2017-155

References

[1] E. Backx. The total temperature in the Longshot wind tunnel, its measurement and evaluation. Technical note 98, von Karman Institute for Fluid Dynamics, April 1974.

[2] K. Bensassi. *Contribution to the numerical modeling of the VKI Longshot hypersonic wind tunnel*. PhD thesis, von Karman Institute for Fluid Dynamics - Université Libre de Bruxelles, January 2014.

[3] H. Bergh and H. Tijdeman. *Theoretical and experimental results for the dynamic response measuring systems*. NLR-TR F.238. 1965.

[4] K. R. Enkenhus and C. Parazzoli. The Longshot free-piston cycle, part I, theory. Technical Note 51, von Karman Institute for Fluid Dynamics, November 1968.

[5] G. Grossir. *Longshot hypersonic wind tunnel flow characterization and boundary layer stability investigations*. PhD thesis, von Karman Institute for Fluid Dynamics - Université Libre de Bruxelles, July 2015.

[6] G. Grossir, Z. Ilich, and O. Chazot. Modeling of the VKI Longshot gun tunnel compression process using a quasi-1D approach. In *33rd AIAA Aerodynamic Measurement Technology and Ground Testing Conference, 2017 AIAA Aviation Forum*, number AIAA-2017-3985, 2017.

[7] P. A. Jacobs. Quasi-one-dimensional modeling of a free-piston shock tunnel. *AIAA Journal*, 32(1):137–145, January 1994.

[8] B. E. Richards and K. R. Enkenhus. Hypersonic testing in the VKI Longshot free-piston tunnel. *AIAA Journal*, 8(6):1020–1025, June 1970.

[9] A. E. Seigel. The theory of high speed guns. In *AGARDograph 91*. NATO, May 1965.

[10] G. Simeonides. The performance of the VKI Longshot hypersonic wind tunnel. Technical Note TN-161, von Karman Institute for Fluid Dynamics, June 1987.